

Three-nodal surface phonons in solid-state materials: Theory and material realizationChengwu Xie,^{1,*} Hongkuan Yuan,^{1,*} Ying Liu,^{2,†} Xiaotian Wang,^{1,‡} and Gang Zhang^{3,§}¹*School of Physical Science and Technology, Southwest University, Chongqing 400715, China*²*School of Materials Science and Engineering, Hebei University of Technology, Tianjin 300130, China*³*Institute of High Performance Computing, Agency for Science, Technology and Research (A*STAR), 138632, Singapore*

(Received 31 August 2021; accepted 28 September 2021; published 11 October 2021)

This year, Liu *et al.* [*Phys. Rev. B* **104**, L041405 (2021)] proposed another class of topological phonons [TPs, i.e., one-nodal surface (NS) phonons], which provides an effective route for realizing one-NS in phonon systems. In this work, based on first-principles calculations and symmetry analysis, we extended the types of NS phonons from one- to three-NS phonons. The existence of three-NS phonons [with three pairs of NS states on the $k_i = \pm \pi$ ($i = x, y, z$) planes in the three-dimensional Brillouin zone (BZ)] is enforced by the combination of twofold screw symmetry and time reversal symmetry. We screened all 230 space groups (SGs) and found nine candidate groups [with the SG numbers (Nos.) 19, 61, 62, 92, 96, 198, 205, 212, and 213] hosting three-NS phonons. Interestingly, with the help of first-principles calculations, we identified $P2_12_12_1$ -type YCuS_2 (SG No. 19), $Pbca$ -type NiAs_2 (SG No. 61), $Pnma$ -type SrZrO_3 (SG No. 62), $P4_12_12$ -type LiAlO_2 (SG No. 92), $P4_32_12$ -type ZnP_2 (SG No. 96), $P2_13$ -type NiSbSe (SG No. 198), $Pa\bar{3}$ -type As_2Pt (SG No. 205), $P4_332$ -type BaSi_2 (SG No. 212), and $P4_132$ -type CsBe_2F_5 (SG No. 213) as realistic materials hosting three-NS phonons. The results of our presented study enrich the class of NS states in phonon systems and provide concrete guidance for searching for three-NS phonons and singular Weyl point phonons in realistic materials.

DOI: [10.1103/PhysRevB.104.134303](https://doi.org/10.1103/PhysRevB.104.134303)**I. INTRODUCTION**

Topological quantum states of matter [1–3] are an important topic in the field of modern condensed-matter physics. Over the past 15 years, we have witnessed the emergence of many types of topological electronic materials, such as topological insulators [4–7], topological crystalline insulators [8–10], topological Kondo insulators [11–13], higher-order topological insulators [14–17], topological semimetals [18–20], and higher-order topological semimetals [21–24]. In particular, the types and numbers of topological semimetals [20] are rapidly increasing. In contrast to Dirac, Weyl, and Majorana fermions, which are allowed in high-energy physics, the types of quasiparticles in topological semimetals [25] are more diverse owing to fewer constraints imposed by the space group (SG) symmetries of the crystal. Based on the dimensionality of the band crossings in the momentum space, the topological semimetals can be classified into nodal point [26–30], nodal line [31–35], and nodal surface (NS) [36–40] semimetals with zero-, one-, and two-dimensional band crossings, respectively.

Three-dimensional topological semimetals with two-dimensional band crossings can host NS states in the Brillouin zone (BZ). Each point on the NS should be a twofold degenerate point with linear band dispersion along the surface normal

direction. Researchers hope that NS semimetals exhibit exotic physical properties, such as stronger quantum oscillations and peculiar plasmon excitations. Wu *et al.* [36] summarized an essential NS state dictated by nonsymmorphic symmetry without spin-orbit coupling (SOC). The existence of a series of NS semimetals in realistic electronic systems has been predicted, including BaVS_3 [40], ZrSiS [41,42], K_6YO_4 [36], FeB_4 [43], Ti_3Al [37], and $\text{X}(\text{MoS})_3$ ($\text{X} = \text{K, Rb, and Cs}$) [44]. However, in general, SOC in electronic materials cannot be ignored; thus, the proposed two-dimensional nonsymmorphic symmetry-enforced NS states in electronic systems will usually be destroyed or reduced to one-dimensional nodal lines when SOC is considered [42]. Moreover, the NS states in some materials are far from the Fermi level and exhibit large energy variations, which hinder their experimental detection.

The proposed topological phonons (TPs) [45,46] have renewed interest in topological quantum states. TPs are a basic kind of boson-type quasiparticles; they are not affected by the Pauli exclusion principle and SOC. Therefore, TPs can normally be observed in spinless phononic systems in all frequency ranges. In addition to the proposed nodal point phonons [47–55] and nodal line phonons [56–64], one-NS phonons [65] [with one pair of NS states on the $k_i = \pm \pi$ ($i = x, y, \text{ or } z$) planes] have been presented by Liu *et al.* based on symmetry analysis and first-principles calculations. The researchers provided a complete list of the one-NS phonons in the 230 SGs and discovered that RbTeAu family materials with SG number (No.) 51 may contain one-NS states (on the $k_x = \pm \pi$ planes). The occurrence of one-NS states is ensured by screw rotation symmetry along the i axis ($i = x, y, \text{ or } z$) and

*These authors contributed equally to this paper.

†ying_liu@hebut.edu.cn

‡xiaotianwang@swu.edu.cn

§zhangg@ihpc.a-star.edu.sg

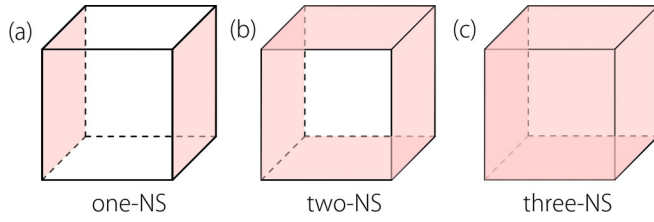


FIG. 1. Schematic diagrams of (a) one-NS, (b) two-NS, (c) and three-NS phonons, respectively.

time-reversal symmetry (\mathcal{T}). Figure 1(a) presents a schematic diagram of one-NS phonons. Moreover, two more types of NS phonons should exist: two- and three-NS phonons, as illustrated in Figs. 1(b) and 1(c), respectively. As shown in Fig. 1(b), two pairs of NSs are localized on two of three $k_i = \pm \pi$ planes ($i = x, y, z$) in the three-dimensional BZ, and they can be named as two-NS phonons. Moreover, as shown in Fig. 1(c), three pairs of NSs are localized on all the $k_i = \pm \pi$ planes in the three-dimensional BZ; one can name them three-NS phonons.

In this study, we extended the class of NS phonons from one- to three-NS phonons. For the three-NS phonons, the NS states are localized on the $k_i = \pm \pi$ ($i = x, y, z$) planes in the three-dimensional BZ. We screened all 230 SGs; the SGs with Nos. 19, 61, 62, 92, 96, 198, 205, 212, and 213 are candidate groups that can obtain three-NS phonons. Because the three-NS phonons in these SGs are symmetry enforced, one can easily achieve three-NS phonons in realistic materials with the previously presented SGs. For example, in this work, we identified $P2_12_12_1$ -type YCuS_2 (SG No. 19), $Pbca$ -type NiAs_2 (SG No. 61), $Pnma$ -type SrZrO_3 (SG No. 62), $P4_12_12$ -type LiAlO_2 (SG No. 92), $P4_32_12$ -type ZnP_2 (SG No. 96), $P2_13$ -type NiSbSe (SG No. 198), $Pa\bar{3}$ -type As_2Pt (SG No. 205), $P4_332$ -type BaSi_2 (SG No. 212), and $P4_132$ -type CsBe_2F_5 (SG No. 213) as realistic materials that can host three-NS phonons.

II. SYMMETRY ANALYSIS OF THREE-NS PHONONS

In this part, we searched all essential NSs, which are only dictated by symmetries, in spinless systems [36]. Such a NS is protected by the combination of \mathcal{T} and twofold screw rotation symmetry (S_{2i}).

Without loss of generalization, we take twofold screw rotation along the z direction as an example: $S_{2z} : (x, y, z) \rightarrow (-x, -y, z + \frac{1}{2})$ with a half translation in the lattice constant along its rotation axis. It also affects the momentum space: $S_{2z} : (k_x, k_y, k_z) \rightarrow (-k_x, -k_y, k_z)$, thereby only preserving the momentum along k_z . Without SOC, $S_{2z}^2 = T_{100} = e^{-ik_z}$, where T_{100} is the translation along the z direction. For \mathcal{T} , in spinless systems, $\mathcal{T}^2 = 1$, which is antiunitary and inverses the momentum \mathbf{k} . Consequently, their combination $\mathcal{T}S_{2z}$ is also antiunitary. Remarkably, on planes where $k_z = \pm\pi$, $(\mathcal{T}S_{2z})^2 = e^{-ik_z}|_{k_z=\pm\pi} = -1$, which suggests Kramer-like degeneracy on these planes. Hence, the phonon bands on the $k_i = \pm\pi$ ($i = x, y, z$) planes must become twofold degenerate, thereby forming three-NS phonons. Furthermore, the presence of three twofold rotation symmetries (i.e., S_{2x} , S_{2y} , and S_{2z}) leads to three pairs of NSs on the planes $k_i = \pm\pi$ ($i =$

x, y, z). In this study, we proposed all the three-NS phonons by searching all 230 SGs in phonon systems. According to the results, the SGs with Nos. 19, 61, 62, 92, 96, 198, 205, 212, and 213 (see Table I) can host three-NS phonons.

III. COMPUTATIONAL DETAILS

First-principles calculations based on density functional theory were performed to study the ground states of $P2_12_12_1$ -type YCuS_2 , $Pbca$ -type NiAs_2 , $Pnma$ -type SrZrO_3 , $P4_12_12$ -type LiAlO_2 , $P4_32_12$ -type ZnP_2 , $P2_13$ -type NiSbSe , $Pa\bar{3}$ -type As_2Pt , $P4_332$ -type BaSi_2 , and $P4_132$ -type CsBe_2F_5 materials, as implemented in the Vienna *ab initio* simulation package. The projector augmented wave method and generalized gradient approximation [66] with Perdew-Burke-Ernzerhof functions were used for the ionic potential and exchange-correlation interaction. In addition, a plane wave cutoff energy of 500 eV was used for the structural relaxation. The following k -mesh samples were used for YCuS_2 , NiAs_2 , SrZrO_3 , LiAlO_2 , ZnP_2 , NiSbSe , As_2Pt , BaSi_2 , and CsBe_2F_5 : $9 \times 7 \times 5$, $5 \times 5 \times 3$, $5 \times 5 \times 5$, $7 \times 7 \times 7$, $7 \times 7 \times 3$, $7 \times 7 \times 7$, $7 \times 7 \times 9$, $9 \times 9 \times 9$, and $5 \times 5 \times 5$, respectively. All these materials are experimentally synthesized materials. The phononic dispersions of the $2 \times 2 \times 1$ YCuS_2 , $2 \times 2 \times 1$ NiAs_2 , $2 \times 1 \times 2$ SrZrO_3 , $2 \times 2 \times 2$ LiAlO_2 , $2 \times 2 \times 1$ ZnP_2 , $2 \times 2 \times 2$ NiSbSe , $2 \times 2 \times 2$ As_2Pt , $2 \times 2 \times 2$ BaSi_2 , and $1 \times 1 \times 1$ CsBe_2F_5 cells were examined with density functional perturbation theory and PHONOPY codes [67].

IV. MATERIALS WITH THREE-NS PHONONS

For phonon systems with SG Nos. 19, 61, 62, the three pairs of NS states appear on the planes $k_y = \pm\pi$, $k_x = \pm\pi$, and $k_z = \pm\pi$, respectively. Obviously, all the three-NS phonons appear in the square-shaped BZ. Moreover, since the NS phonons on $k_i = \pi$ and $k_i = -\pi$ ($i = x, y, z$) are the same, we mainly discuss the NS phonons on $k_i = \pi$ in this section. Some realistic materials were selected as examples to demonstrate that they host three-NS phonons: $P2_12_12_1$ -type YCuS_2 (SG No. 19) can be prepared [68] by fusing the high-purity elements in evacuated quartz ampoules; Murray and Heyding [69] prepared $Pbca$ -type NiAs_2 (SG No. 61) by heating the elements in sealed evacuated Vycor tubes; $Pnma$ -type SrZrO_3 powders (SG No. 62) were prepared with the polymeric precursor method by Cavalcante *et al.* [70]. The crystal structures of these three materials are shown in Fig. 2. They are completely relaxed; their theoretically determined lattice constants and the previously published experimentally determined data are listed in Table II.

The phonon dispersions of YCuS_2 , NiAs_2 , and SrZrO_3 along the Γ - X - S - Y - Γ - Z - S - X - U - Z - T - Y - S - R paths [see Fig. 3(a)] are shown in Figs. 3(b)–3(d), respectively. Three regions (highlighted in red, yellow, and green boxes) are of interests in this study. The enlarged figures of the phonon dispersions of YCuS_2 , NiAs_2 , and SrZrO_3 in the three regions are shown in Figs. 4(a), 4(c) and 4(e), respectively. All the phonon bands along the S - X - U , U - Z - T , and T - Y - S planes have twofold degeneracy. To explain this in more detail, some symmetry lines [i.e., a - P - a' , b - Q - b' , and c - N - c' ; see Fig. 3(a)] are selected; they are perpendicular to the S - X ,

TABLE I. A complete list of three-NS phonons in 230 SGs. The first and second columns present the SG numbers and SG symbols, the third column lists the NSs along the symmetry paths, and the fourth column presents the corresponding realistic materials. For SGs with Nos. 19, 61, 62, three perpendicular NS states appear on the BZ boundary planes (such as BZ_{TYS} , BZ_{SXU} , and BZ_{UZT}). The TYS , SXU , UZT are the high-symmetry paths in the $k_y = \pi$, $k_x = \pi$, and $k_z = \pi$ planes, respectively. For SGs with Nos. 92 and 96, we exhibit two NS states on BZ_{ZRA} and BZ_{MXR} boundary planes (i.e., $k_z = \pi$ and $k_y = \pi$). Equivalent NS state on the $k_x = \pi$ plane is not given in this table. For SGs with Nos. 198, 205, 212, 213, we only show one NS state on the BZ_{RXM} boundary plane ($k_y = \pi$). Equivalent NS states on $k_x = \pi$ and $k_z = \pi$ planes are not given in this table.

Space group numbers	Space group symbols	Nodal surfaces	Realistic materials
19	$P2_12_12_1$	BZ_{TYS} , BZ_{SXU} , and BZ_{UZT}	YCuS ₂
61	$Pbca$	BZ_{TYS} , BZ_{SXU} , and BZ_{UZT}	NiAs ₂
62	$Pnma$	BZ_{TYS} , BZ_{SXU} , and BZ_{UZT}	SrZrO ₃
92	$P4_12_12$	BZ_{ZRA} , and BZ_{MXR}	LiAlO ₂
96	$P4_32_12$	BZ_{ZRA} , and BZ_{MXR}	ZnP ₂
198	$P2_13$	BZ_{RXM}	NiSbSe
205	$Pa\bar{3}$	BZ_{RXM}	As ₂ Pt
212	$P4_332$	BZ_{RXM}	BaSi ₂
213	$P4_132$	BZ_{RXM}	CsBe ₂ F ₅

T - Z , and Y - T symmetry lines, respectively. Subsequently, we calculate the phonon dispersions along the a - P - a' , b - Q - b' , and c - N - c' paths; the results are presented in Figs. 4(b), 4(d) and 4(f), respectively. Evidently, the points (highlighted by red circles) at the P , Q , and N symmetry points are twofold degenerate and have linear band dispersions. In addition, twofold Kramer-like degeneracy occurs at every point on the S - X - U , U - Z - T , and T - Y - S planes, thereby forming three NSs on the $k_i = \pi$ ($i = x, y, z$) planes. These density functional theory results agree well with the arguments in Sec. II.

The NSs belong to essential nodal nodal surfaces indicated by nonsymmorphic symmetry. As shown in Ref. [71], such 2D band crossings are of twisted Möbius strip band structure, implying the presence of a nontrivial \mathbb{Z}_2 topological charge. That is to say, provided the symmetry is preserved, the band crossings only disappear in pairs. To illustrate it, we construct

a model for generic band crossing P on path X - S ; it can be characterized by a two-band effective model. Most specifically, the little point group at P point belongs to C_{2v} , which is generated by C_{2x} , M_z , and together with space-time inversion symmetry \mathcal{PT} . Thus, there are two pairs of 1D irreducible representations, namely $\{R_2, R_4\}$, $\{R_6, R_8\}$, in which the generating elements take the following form,

$$C_{2x} = \sigma_x, M_z = \pm \sigma_0, \mathcal{PT} = \sigma_x \mathcal{K}, \quad (1)$$

with \mathcal{K} the complex conjugation. Thereby, one could derive the effective model of two bands as

$$\mathcal{H}(k) = (c_0 + c_1 k_y) \sigma_0 + k_x (c_2 \sigma_x + c_3 \sigma_y), \quad (2)$$

with σ 's the Pauli matrix. The overall energy shift which is linear to σ_0 can be neglected; it has no effects on its topological. Thereby, such a model performs linear band crossings at the boundary of BZ, as shown in Figs. 4(b), 4(d) and 4(f). According to the nature of \mathbb{Z}_2 topological charge, if we double the Hamiltonian $\mathcal{H}(k) \otimes \sigma_0$, with symmetry taking the forms of $\{C_{2x}, M_z, \mathcal{PT}\} \otimes \sigma_0$, the four-band model is gapped out by symmetry preserving terms. For example, the one term $\Delta_0 \sigma_0 \otimes \sigma_x$ is allowed, but it gaps the band crossing.

In the next step, some realistic materials with SG Nos. 92 and 96 and three-NS phonons are presented. The first example is $P4_12_12$ -type LiAlO₂ (SG No. 92); Remeika and Ballman [72] prepared these single crystals from a flux. The

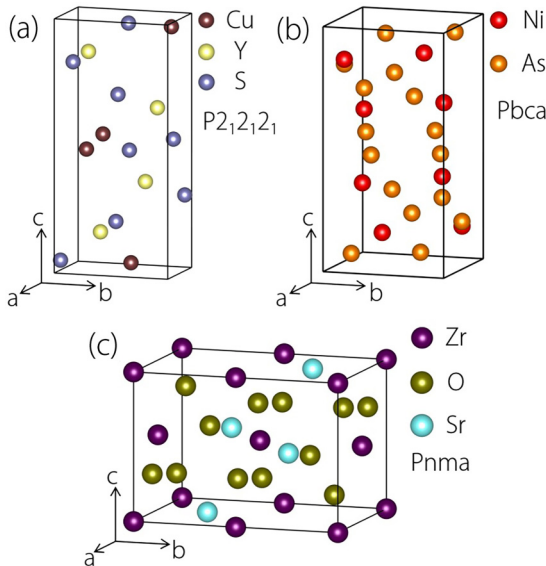


FIG. 2. Crystal structures of $P2_12_12_1$ -type YCuS₂ (SG No. 19), $Pbca$ -type NiAs₂ (SG No. 61), and $Pnma$ -type SrZrO₃ (SG No. 62), respectively.

TABLE II. Theoretically and experimentally determined lattice constants of YCuS₂, NiAs₂, and SrZrO₃.

Materials	Theoretical lattice constants	Experimental lattice constants [68–70]
YCuS ₂	$a = 3.96 \text{ \AA}$, $b = 6.26 \text{ \AA}$, $c = 13.48 \text{ \AA}$	$a = 3.97 \text{ \AA}$, $b = 6.27 \text{ \AA}$, $c = 13.38 \text{ \AA}$
NiAs ₂	$a = 5.80 \text{ \AA}$, $b = 5.89 \text{ \AA}$, $c = 11.50 \text{ \AA}$	$a = 5.77 \text{ \AA}$, $b = 5.83 \text{ \AA}$, $c = 11.41 \text{ \AA}$
SrZrO ₃	$a = 5.91 \text{ \AA}$, $b = 8.29 \text{ \AA}$, $c = 5.84 \text{ \AA}$	$a = 5.81 \text{ \AA}$, $b = 8.19 \text{ \AA}$, $c = 5.79 \text{ \AA}$

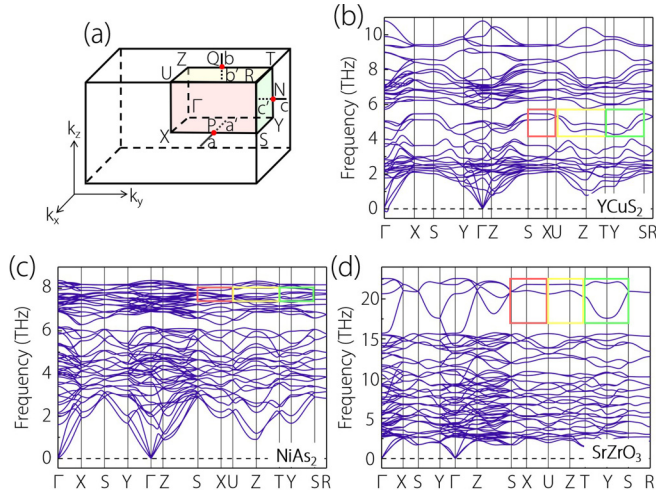


FIG. 3. (a) Three-dimensional BZ and symmetry points. Three NS states are localized on the $k_i = \pi$ ($i = x, y, z$) planes in three-dimensional BZ. (b)–(d) Calculated phonon dispersions of YCuS_2 , NiAs_2 , and SrZrO_3 , respectively. NS regions (i.e., $\text{BZ}_{\Gamma\text{YS}}$, BZ_{SXU} , and BZ_{UZT}) are highlighted in green, red, and yellow boxes, respectively.

second example is $P4_32_12$ -type ZnP_2 (SG No. 96). Researchers [73] have reported that ZnP_2 crystals can exist in an enantiomorphic form with SG $P4_32_12 = D_4^8$. The theoretically determined and previously published experimental lattice constants are shown in Table III. The crystal struc-

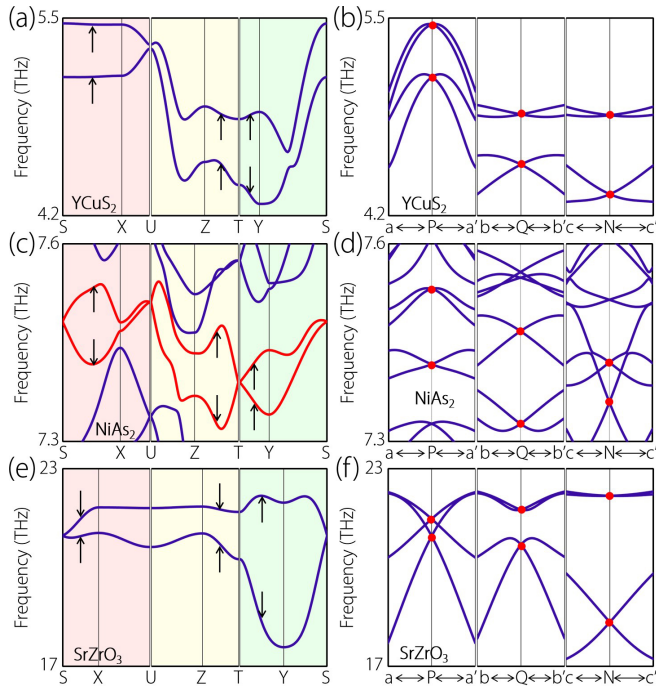


FIG. 4. (a),(c),(e) Enlarged phonon dispersions of three regions [see Figs. 3(b)–3(d)] of YCuS_2 , NiAs_2 , and SrZrO_3 , respectively. (b),(d),(f) Phonon dispersions along a (0.70, 0.25, 0.00) $-P$ (0.50, 0.25, 0.00) $-a'$ (0.30, 0.25, 0.00), b (0.00, 0.25, 0.7) $-Q$ (0.00, 0.25, 0.5) $-b'$ (0.00, 0.25, 0.3), and c (0.00, 0.7, 0.25) $-N$ (0.00, 0.5, 0.25) $-c'$ (0.00, 0.3, 0.25), respectively. All points at P , Q , and N points are twofold degenerate with linear phonon band dispersions.

TABLE III. Theoretically and experimentally determined lattice constants of LiAlO_2 and ZnP_2 .

Materials	Theoretical lattice constants	Experimental lattice constants [72,73]
LiAlO_2	$a = b = 5.21 \text{ \AA}$, $c = 6.30 \text{ \AA}$	$a = b = 5.17 \text{ \AA}$, $c = 6.59 \text{ \AA}$
ZnP_2	$a = b = 5.06 \text{ \AA}$, $c = 18.53 \text{ \AA}$	$a = b = 5.10 \text{ \AA}$, $c = 18.62 \text{ \AA}$

tures of the two materials are shown in Figs. 5(a) and 5(b). The phonon dispersions of the two materials along the Γ - X - M - Γ - Z - R - A - M - X - R paths [see Fig. 5(c)] are presented in Figs. 5(d) and 5(e). To examine the three-NS phonons in these two materials, we only focused on two paths: Z - R - A and M - X - R , which are highlighted in yellow and green boxes in Figs. 5(d) and 5(e), respectively. The enlarged phonon dispersions of these two regions for LiAlO_2 and ZnP_2 are shown in Figs. 6(a) and 6(c), respectively. All the phonon bands along the Z - R - A and M - X - R paths are twofold degenerate. To present examples, we select two symmetry points N and Q on the $k_y = \pi$ and $k_z = \pi$ planes, respectively. We construct the two paths b - Q - b' and c - N - c' , which vertically pass through the $k_z = \pi$ and $k_y = \pi$ planes, respectively. The obtained phonon dispersions along the b - Q - b' and c - N - c' paths for LiAlO_2 and ZnP_2 are shown in Figs. 6(b) and 6(d), respectively. There are two twofold degenerate points at Q and N , which represent the NS states on the $k_z = \pi$ and $k_y = \pi$ planes. Because LiAlO_2 and ZnP_2 with SG Nos. 92 and 96 host four-fold screw rotation, $S_{4z} = \{C_{4z}|00\frac{1}{2}\}$, there should be NSs on the $k_x = \pi$ planes.

Finally, some realistic materials with SG Nos. 198, 205, 212, and 213 are presented, which host three-NS phonons. The first example is $P2_13$ -type NiSbSe (SG No. 198). It was

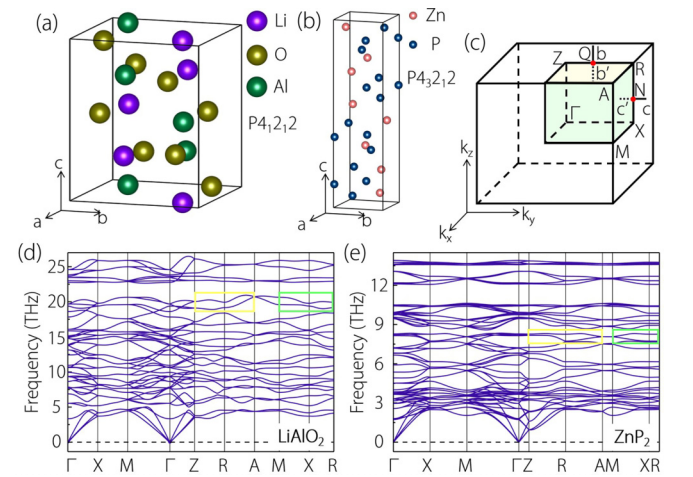


FIG. 5. (a),(b) Crystal structures of $P4_12_12$ -type LiAlO_2 (SG No. 92) and $P4_32_12$ -type ZnP_2 (SG No. 96), respectively; (c) Three-dimensional BZ and symmetry points. Three NS states are localized on $k_i = \pi$ ($i = x, y, z$) planes in three-dimensional BZ. (b)–(d) Calculated phonon dispersions of LiAlO_2 and ZnP_2 , respectively. NS regions (i.e., BZ_{MXR} and BZ_{ZRA}) are highlighted in green and yellow boxes, respectively.

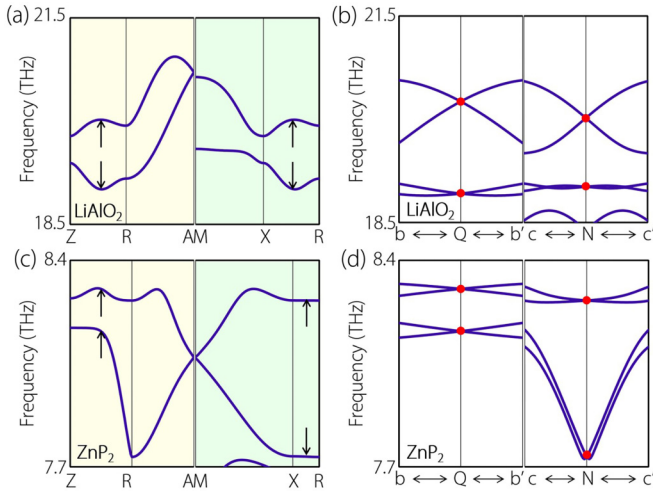


FIG. 6. (a),(c) Enlarged phonon dispersions of two regions [see Figs. 5(d) and 5(e)] of LiAlO_2 and ZnP_2 , respectively. (b),(d) Phonon dispersions along b (0.00, 0.25, 0.7) $-N$ (0.00, 0.25, 0.5) $-b'$ (0.00, 0.25, 0.3), and c (0.00, 0.7, 0.25) $-Q$ (0.00, 0.5, 0.25) $-c'$ (0.00, 0.3, 0.25), respectively. All the points at the Q and N points are twofold degenerate points with linear phonon band dispersions.

prepared by letting powders of binary nickel chalcogenides react with the respective pnictogen component in evacuated sealed silica tubes [74]. The second example is $Pa\bar{3}$ -type As_2Pt (SG No. 205). Ramsdell [75] produced artificial PtAs_2 , which is identical to natural sperrylite. The third example is $P4_332$ -type BaSi_2 (SG No. 212). This compound is an interesting material [76] that can host three types of polymorphs (orthorhombic, trigonal, and cubic crystal classes with $Pnma$, $P\bar{3}m1$, and $P4_332$ SGs) at up to 40 kbar and 1000 °C. $P4_332$ -type BaSi_2 represents one kind of the high-pressure phases. The fourth example is $P4_132$ -type CsBe_2F_5 (SG No. 213). Le Fur and Aléonard [77] dissolved Cs_2CO_2 carbonate in a hydrofluoric solution containing excess BeF_2 . A single CsBe_2F_5 crystal can be obtained via evaporation at 55 °C. The crystal structures of these materials are shown in Fig. 7. We

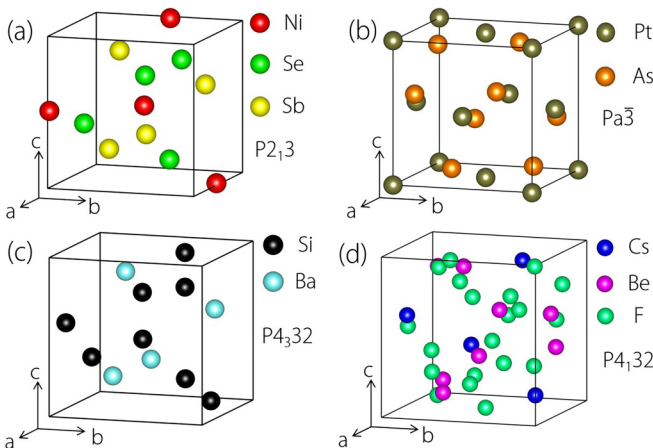


FIG. 7. (a)–(d) Crystal structures of $P2_13$ -type NiSbSe (SG No. 198), $Pa\bar{3}$ -type As_2Pt (SG No. 205), $P4_332$ -type BaSi_2 (SG No. 212), and $P4_132$ -type CsBe_2F_5 (SG No. 213), respectively.

TABLE IV. Theoretically and experimentally determined lattice constants of NiSbSe , As_2Pt , BaSi_2 , and CsBe_2F_5 .

Materials	Theoretical lattice constants	Experimental lattice constants [74–77]
NiSbSe	$a = b = c = 6.13 \text{ \AA}$	$a = b = c = 6.08 \text{ \AA}$
As_2Pt	$a = b = c = 6.06 \text{ \AA}$	$a = b = c = 5.92 \text{ \AA}$
BaSi_2	$a = b = c = 6.77 \text{ \AA}$	$a = b = c = 6.71 \text{ \AA}$
CsBe_2F_5	$a = b = c = 8.06 \text{ \AA}$	$a = b = c = 7.93 \text{ \AA}$

determined their lattice constants with structural-relaxation calculations (see Fig. 7 and Table IV).

We calculated the phonon dispersions of NiSbSe , As_2Pt , BaSi_2 , and CsBe_2F_5 along the symmetry paths $\Gamma-X-M-\Gamma-R-X-M$ [see Fig. 8(a)]; the results are shown in Figs. 8(b)–8(d). Let us focus on the twofold degenerate phonon bands along the $R-X-M$ paths [see Figs. 9(a), 9(c) 9(e), and 9(g)]. To prove that these bands are degenerated, we chose the path $a-P-a'$ that vertically passes through the $k_y = \pi$ plane. The obtained phonon dispersions along the $a-P-a'$ path for these materials are shown in Figs. 9(b), 9(d) 9(f), and 9(h), respectively. There are two evident twofold degenerate points at P with linear band dispersions. We can conclude that a NS phonon exists on the $k_y = \pi$ plane on which the two low-energy phonon bands cross linearly. Owing to $C_{3,111}$ symmetry, equivalent NS phonons can be found on the $k_x = \pi$ and $k_y = \pi$ planes. We would like to point out that although symmetry requires the occurrence of three-NS phonons and limits the possible positions on the $k_i = \pm \pi$ ($i = x, y, z$) planes, it does not limit the frequencies and dispersions of three-NS phonons.

V. SUMMARY AND REMARKS

In conclusion, according to the symmetry analysis results, there are three-NS phonons in the SGs with SG Nos. 19, 61, 62, 92, 96, 198, 205, 212, and 213 of the 230 SGs. More interestingly, by performing first-principles calculations, we discovered that the realistic materials $P2_12_1$ -type YCuS_2 (SG No. 19), $Pbca$ -type NiAs_2 (SG No. 61), $Pnma$ -type SrZrO_3 (SG No. 62), $P4_12_1$ -type LiAlO_2 (SG No. 92), $P4_32_1$ -type ZnP_2 (SG No. 96), $P2_13$ -type NiSbSe (SG No. 198), $Pa\bar{3}$ -type As_2Pt (SG No. 205), $P4_332$ -type BaSi_2 (SG No. 212), and $P4_132$ -type CsBe_2F_5 (SG No. 213) include three-NS phonons in their phonon dispersions.

We present the following remarks: (i) Because phonons obey Bose-Einstein statistics and are not limited by the Fermi energy, three pairs of NSs in the phonon system may be more common in realistic materials. (ii) Unlike fermions in electronic systems with heavy elements, SOC can be neglected for TPs in phonon systems. Hence, three pairs of NSs in phonon systems can be considered real NS states without SOC-induced gaps. (iii) Although three-NS phonons in SGs 19, 61, 62, 92, 96, 198, 205, 212, and 213 can be determined by the combination of twofold screw symmetry and time reversal symmetry, the frequencies and dispersions of three-NS phonons are not limited. (iv) One may ask what is the difference between three pairs of NS and one pair of (two

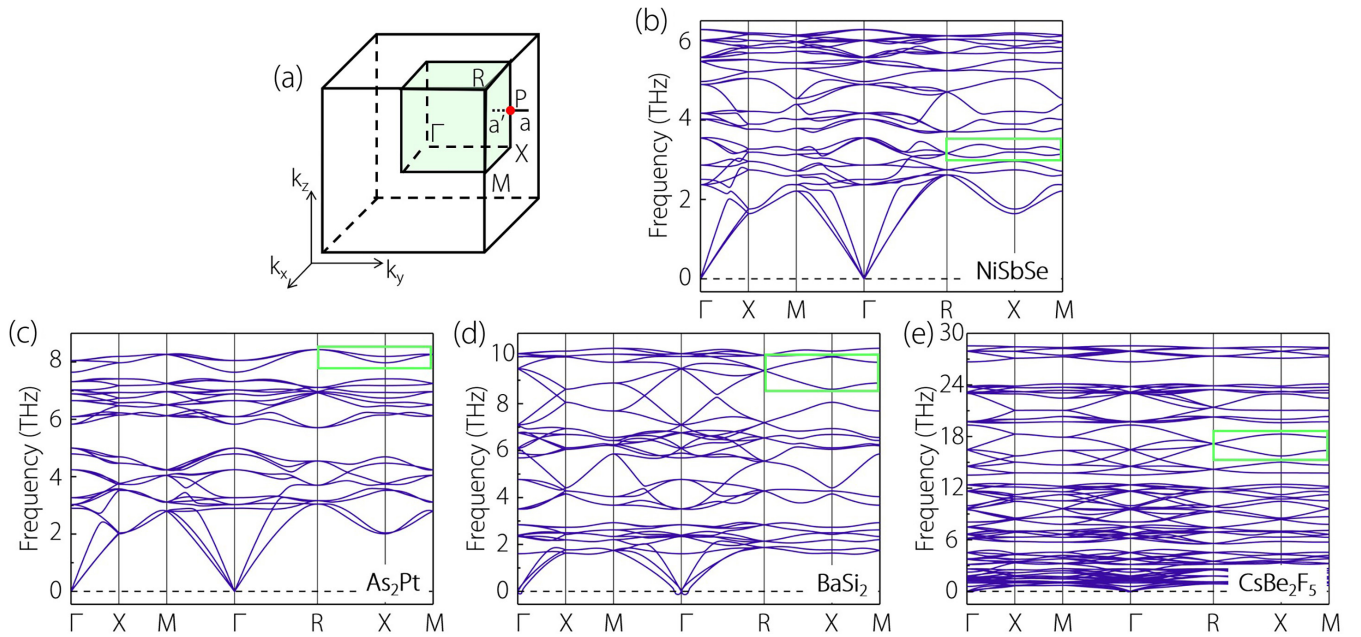


FIG. 8. (a) Three-dimensional BZ and symmetry points. Three NS states are localized on $k_i = \pi$ ($i = x, y, z$) planes in three-dimensional BZ. (b)–(e) Calculated phonon dispersions of NiSbSe, As₂Pt, BaSi₂, and CsBe₂F₅ materials, respectively. NS region (BZ_{RXM}) is highlighted in a green box.

pairs of) NS states? As we know, constrained by the no-go theorem, among all the Weyl semimetals [78] discovered in experiments before 2019, Weyl points always occur in pairs in the momentum space, without exception. Interestingly, in 2019, as demonstrated by Yu *et al.* [79], the three pairs of NS states are good platforms for realizing a singular Weyl

point by circumventing the no-go theorem. However, for one and two pair(s) of NSs, although Weyl points and NS states can coexist, there must be more than one Weyl point in the BZ. Fortunately, in this year, Ma *et al.* [78] observed a singular Weyl point surrounded by three pairs of NSs in PtGa with SG No. 198 in an experiment. (v) We would like

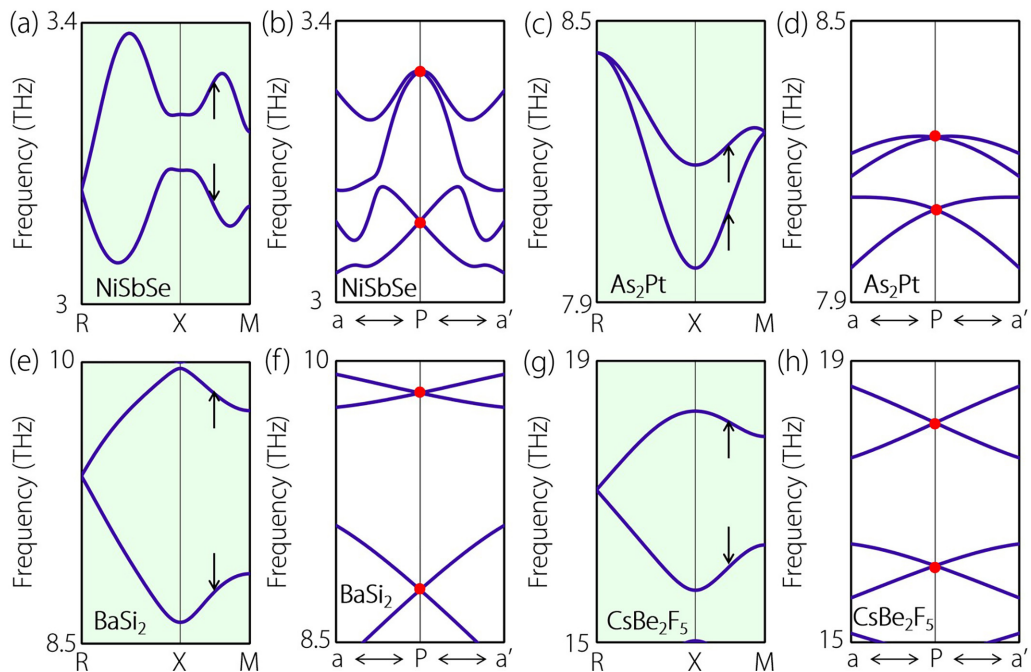


FIG. 9. (a),(c),(e),(g) Enlarged phonon dispersions of the R - X - M path [see Figs. 8(b)–8(e)] of As₂Pt, BaSi₂, and CsBe₂F₅ materials, respectively. (b),(d),(f),(h) Phonon dispersions along the a (0.00, 0.70, 0.25)– P (0.00, 0.50, 0.25)– a' (0.00, 0.30, 0.25) path. All points at the P symmetry point are twofold degenerate points with linear phonon band dispersions [indicated by red circles in (b), (d), (f), and (h)].

to point out that another class of NS (named class-I NS in Ref. [36]) has been reported in carbon allotropes [80] in the absence of SOC. The condition for the presence of class-I NS in carbon allotropes is quite stringent: Besides the \mathcal{PT} and sublattice symmetry, its appearance also requires regions in BZ with inverted band orderings (different \mathbb{Z}_2 indices). However, the occurrence of one, two, three pair(s) of NSs [65] (named class-II NSs in Ref. [36]) is solely guaranteed by symmetry. Hence, this makes it easier to search for candidate materials with class-II NS phonons by analyzing the space groups. The candidate materials with class-II NS phonons presented in this work are selected from the Materials

Project database [81]. It is hoped that the three-NS phonons in these realistic materials can be confirmed in experiments soon.

ACKNOWLEDGMENTS

X.W. thanks Prof. Zhi-Ming Yu for his help regarding to this paper. Y.L. is grateful for the support from the Nature Science Foundation of Hebei Province (No. A2021202002). X.W. and H.Y. are grateful for support from the National Natural Science Foundation of China (Grants No. 51801163 and No. 11874306).

-
- [1] F. D. M. Haldane, *Rev. Mod. Phys.* **89**, 040502 (2017).
- [2] C.-K. Chiu, J. C. Y. Teo, A. P. Schnyder, and S. Ryu, *Rev. Mod. Phys.* **88**, 035005 (2016).
- [3] N. Goldman, J. C. Budich, and P. Zoller, *Nat. Phys.* **12**, 639 (2016).
- [4] M. Z. Hasan and C. L. Kane, *Rev. Mod. Phys.* **82**, 3045 (2010).
- [5] X.-L. Qi and S.-C. Zhang, *Rev. Mod. Phys.* **83**, 1057 (2011).
- [6] L. Fu, C. L. Kane, and E. J. Mele, *Phys. Rev. Lett.* **98**, 106803 (2007).
- [7] Y. Tokura, K. Yasuda, and A. Tsukazaki, *Nat. Rev. Phys.* **1**, 126 (2019).
- [8] L. Fu, *Phys. Rev. Lett.* **106**, 106802 (2011).
- [9] Y. Ando and L. Fu, *Annu. Rev. Condens. Matter Phys.* **6**, 361 (2015).
- [10] T. H. Hsieh, H. Lin, J. Liu, W. Duan, A. Bansil, and L. Fu, *Nat. Commun.* **3**, 982 (2012).
- [11] M. Dzero, K. Sun, V. Galitski, and P. Coleman, *Phys. Rev. Lett.* **104**, 106408 (2010).
- [12] M. Dzero, J. Xia, V. Galitski, and P. Coleman, *Annu. Rev. Condens. Matter Phys.* **7**, 249 (2016).
- [13] M. Dzero, K. Sun, P. Coleman, and V. Galitski, *Phys. Rev. B* **85**, 045130 (2012).
- [14] F. Schindler, A. M. Cook, M. G. Vergniory, Z. Wang, S. S. P. Parkin, B. A. Bernevig, and T. Neupert, *Sci. Adv.* **4**, eaat0346 (2018).
- [15] E. Khalaf, *Phys. Rev. B* **97**, 205136 (2018).
- [16] M. Ezawa, *Phys. Rev. Lett.* **120**, 026801 (2018).
- [17] R. Chen, C.-Z. Chen, J.-H. Gao, B. Zhou, and D.-H. Xu, *Phys. Rev. Lett.* **124**, 036803 (2020).
- [18] A. A. Burkov, *Nat. Mater.* **15**, 1145 (2016).
- [19] H. Gao, J. W. F. Venderbos, Y. Kim, and A. M. Rappe, *Annu. Rev. Mater. Res.* **49**, 153 (2019).
- [20] B. Q. Lv, T. Qian, and H. Ding, *Rev. Mod. Phys.* **93**, 025002 (2021).
- [21] D. Călugăru, V. Juričić, and B. Roy, *Phys. Rev. B* **99**, 041301(R) (2019).
- [22] Z. Zhang, Z.-M. Yu, and S. A. Yang, *Phys. Rev. B* **103**, 115112 (2021).
- [23] W. Wu, Z.-M. Yu, X. Zhou, Y. X. Zhao, and S. A. Yang, *Phys. Rev. B* **101**, 205134 (2020).
- [24] Z.-M. Yu, W. K. Wu, X.-L. Sheng, Y. X. Zhao, and S. Y. A. Yang, *Phys. Rev. B* **99**, 121106(R) (2019).
- [25] Z.-M. Yu, Z. Zhang, G.-B. Liu, W. Wu, X.-P. Li, R.-W. Zhang, S. A. Yang, and Y. Yao, [arXiv:2102.01517v3](https://arxiv.org/abs/2102.01517v3).
- [26] N. P. Armitage, E. J. Mele, and A. Vishwanath, *Rev. Mod. Phys.* **90**, 015001 (2018).
- [27] Q. D. Gibson, L. M. Schoop, L. Muechler, L. S. Xie, M. Hirschberger, N. P. Ong, R. Car, and R. J. Cava, *Phys. Rev. B* **91**, 205128 (2015).
- [28] B.-J. Yang and N. Nagaosa, *Nat. Commun.* **5**, 4898 (2014).
- [29] B. Yan and C. Felser, *Annu. Rev. Condens. Matter Phys.* **8**, 337 (2017).
- [30] A. A. Soluyanov, D. Gresch, Z. Wang, Q. Wu, M. Troyer, X. Dai, and B. A. Bernevig, *Nature (London)* **527**, 495 (2015).
- [31] C. Fang, Y. Chen, H.-Y. Kee, and L. Fu, *Phys. Rev. B* **92**, 081201(R) (2015).
- [32] Q. Xu, R. Yu, Z. Fang, X. Dai, and H. Weng, *Phys. Rev. B* **95**, 045136 (2017).
- [33] T. He, X. Zhang, Y. Liu, X. Dai, G. Liu, Z.-M. Yu, and Y. Yao, *Phys. Rev. B* **102**, 075133 (2020).
- [34] L. Jin, X. M. Zhang, Y. Liu, X. F. Dai, X. N. Shen, L. Y. Wang, and G. D. Liu, *Phys. Rev. B* **102**, 125118 (2020).
- [35] H. Zhang, X. Zhang, T. He, X. Dai, Y. Liu, G. Liu, L. Wang, and Y. Zhang, *Phys. Rev. B* **102**, 155116 (2020).
- [36] W. Wu, Y. Liu, S. Li, C. Zhong, Z.-M. Yu, X.-L. Sheng, Y. X. Zhao, and S. A. Yang, *Phys. Rev. B* **97**, 115125 (2018).
- [37] X. M. Zhang, Z.-M. Yu, Z. M. Zhu, W. K. Wu, S.-S. Wang, X.-L. Sheng, and S. A. Yang, *Phys. Rev. B* **97**, 235150 (2018).
- [38] B.-B. Fu, C.-J. Yi, T.-T. Zhang, M. Caputo, J.-Z. Ma, X. Gao, B. Q. Lv, L.-Y. Kong, Y.-B. Huang, P. Richard, M. Shi, V. N. Strocov, C. Fang, H.-M. Weng, Y.-G. Shi, T. Qian, and H. Ding, *Sci. Adv.* **5**, eaau6459 (2019).
- [39] S. Z. Chen, S. Li, Y. Chen, and W. Duan, *Nano Lett.* **20**, 5400 (2020).
- [40] Q.-F. Liang, J. Zhou, R. Yu, Z. Wang, and H. Weng, *Phys. Rev. B* **93**, 085427 (2016).
- [41] A. Topp, R. Queiroz, A. Grüneis, L. Muechler, A. W. Rost, A. Varykhalov, D. Marchenko, M. Krivenkov, F. Rodolakis, J. L. McChesney, B. V. Lotsch, L. M. Schoop, and C. R. Ast, *Phys. Rev. X* **7**, 041073 (2017).
- [42] C. Chen, X. Xu, J. Jiang, S.-C. Wu, Y. P. Qi, L. X. Yang, M. X. Wang, Y. Sun, N. B. M. Schröter, H. F. Yang, L. M. Schoop, Y. Y. Lv, J. Zhou, Y. B. Chen, S. H. Yao, M. H. Lu, Y. F. Chen, C. Felser, B. H. Yan, Z. K. Liu, and Y. L. Chen, *Phys. Rev. B* **95**, 125126 (2017).
- [43] F. Zhou, Y. Liu, J. H. Wang, M. Q. Kuang, T. Yang, H. Chen, X. T. Wang, and Z. X. Cheng, *Phys. Rev. Materials* **5**, 074201 (2021).

- [44] T. Yang and X. Zhang, *J. Mater. Chem. C* **8**, 9046 (2020).
- [45] O. Stenull, C. L. Kane, and T. C. Lubensky, *Phys. Rev. Lett.* **117**, 068001 (2016).
- [46] Y. Liu, X. Chen, and Y. Xu, *Adv. Funct. Mater.* **30**, 1904784 (2019).
- [47] T. T. Zhang, Z. D. Song, A. Alexandradinata, H. M. Weng, C. Fang, L. Lu, and Z. Fang, *Phys. Rev. Lett.* **120**, 016401 (2018).
- [48] J. X. Li, Q. Xie, S. Ullah, R. H. Li, H. Ma, D. Z. Li, Y. Y. Li, and X.-Q. Chen, *Phys. Rev. B* **97**, 054305 (2018).
- [49] H. Miao, T. T. Zhang, L. Wang, D. Meyers, A. H. Said, Y. L. Wang, Y. G. Shi, H. M. Weng, Z. Fang, and M. P. M. Dean, *Phys. Rev. Lett.* **121**, 035302 (2018).
- [50] B. W. Xia, R. Wang, Z. J. Chen, Y. J. Zhao, and H. Xu, *Phys. Rev. Lett.* **123**, 065501 (2019).
- [51] Q.-B. Liu, Y. Qian, H.-H. Fu, and Z. Wang, *Npj Comput. Mater.* **6**, 95 (2020).
- [52] Q.-B. Liu, Z. Wang, and H.-H. Fu, *Phys. Rev. B* **103**, L161303 (2021).
- [53] J. Liu, W. Hou, E. Wang, S. Zhang, J.-T. Sun, and S. Meng, *Phys. Rev. B* **100**, 081204(R) (2019).
- [54] Y. J. Jin, Z. J. Chen, X. L. Xiao, and H. Xu, *Phys. Rev. B* **103**, 104101 (2021).
- [55] J.-Y. You, X.-L. Sheng, and G. Su, *Phys. Rev. B* **103**, 165143 (2021).
- [56] G. Liu, Y. J. Jin, Z. G. Chen, and H. Xu, *Phys. Rev. B* **104**, 024304 (2021).
- [57] B. Zheng, B. Xia, R. Wang, Z. Chen, J. Zhao, Y. Zhao, and H. Xu, *Phys. Rev. B* **101**, 100303(R) (2020).
- [58] Y. J. Jin, Z. J. Chen, B. W. Xia, Y. J. Zhao, R. Wang, and H. Xu, *Phys. Rev. B* **98**, 220103(R) (2018).
- [59] R. Y. Wang, Z. J. Chen, Z. Q. Huang, B. W. Xia, and H. Xu, *Phys. Rev. Materials* **5**, 084202 (2021).
- [60] B. B. Zheng, F. Y. Zhan, X. Z. Wu, R. Wang, and J. Fan, *Phys. Rev. B* **104**, L060301 (2021).
- [61] J. J. Zhu, W. K. Wu, J. Z. Zhao, Hao. Chen, L. F. Zhang, and S. Y. A. Yang, [arXiv:2104.14816](https://arxiv.org/abs/2104.14816).
- [62] Q.-B. Liu, H.-H. Fu, and R. Q. Wu, *Phys. Rev. B* **104**, 045409 (2021).
- [63] J. Li, J. Liu, S. A. Baronett, M. Liu, L. Wang, R. Li, Y. Chen, D. Li, Q. Zhu, and X.-Q. Chen, *Nat. Commun.* **12**, 1204 (2021).
- [64] T. T. Zhang, H. Miao, Q. Wang, J. Q. Lin, Y. Cao, G. Fabbris, A. H. Said, X. Liu, H. C. Lei, Z. Fang, H. M. Weng, and M. P. M. Dean, *Phys. Rev. Lett.* **123**, 245302 (2019).
- [65] Q.-B. Liu, Z.-Q. Wang, and H.-H. Fu, *Phys. Rev. B* **104**, L041405 (2021).
- [66] J. P. Perdew, K. Burke, and M. Ernzerhof, *Phys. Rev. Lett.* **77**, 3865 (1996).
- [67] A. Togo and I. Tanaka, *Scr. Mater.* **108**, 1 (2015).
- [68] L. D. Gulay, V. Ya. Shemet, and I. D. Olekseyuk, *J. Alloys Compd.* **388**, 59 (2005).
- [69] J. J. Murray and R. D. Heyding, *Can. J. Chem.* **45**, 2675 (1967).
- [70] L. S. Cavalcante, A. Z. Simoes, E. Longo, J. C. Sczancoski, R. Erlo, M. T. Escote, V. M. Longo, and J. A. Varela, *Solid State Sci.* **9**, 1020 (2007).
- [71] Y. X. Zhao and A. P. Schnyder, *Phys. Rev. B* **94**, 195109 (2016).
- [72] J. P. Remeika and A. A. Ballman, *Appl. Phys. Lett.* **5**, 180 (1964).
- [73] K. B. Aleinikova, A. I. Kozlov, S. G. Kozlova, and V. V. Sobolev, *Phys. Solid State*, **44**, 1257 (2002).
- [74] A. J. Foecker and W. Jeitschko, *J. Sol. State. Chem.* **162**, 69 (2001).
- [75] L. S. Ramsdell, *Am. Mineral.* **10**, 281 (1925).
- [76] J. Evers, *J. Solid State Chem.* **32**, 77 (1980).
- [77] Y. L. Fur and S. Aléonard, *Acta Crystallogr.* **28**, 2115 (1972).
- [78] J.-Z. Ma, Q.-S. Wu, M. Song, S.-N. Zhang, E. B. Guedes, S. A. Ekahana, M. Krivenkov, M. Y. Yao, S.-Y. Gao, W.-H. Fan, T. Qian, H. Ding, N. C. Plumb, M. Radovic, J. H. Dil, Y.-M. Xiong, K. Manna, C. Felser, O. V. Yazyev, and M. Shi, *Nat. Commun.* **12**, 3994 (2021).
- [79] Z.-M. Yu, W. Wu, Y. X. Zhao, and S. A. Yang, *Phys. Rev. B* **100**, 041118(R) (2019).
- [80] C. Zhong, Y. Chen, Y. Xie, S. A. Yang, M. L. Cohen, and S. Zhang, *Nanoscale* **8**, 7232 (2016).
- [81] <https://materialsproject.org>.